Anal. Chem. **2004,** *76,* 6229−6238

The Nanopore Electrode

Bo Zhang, Yanhui Zhang, and Henry S. White*

Departments of Chemistry, University of Utah, Salt Lake City, Utah 84112

The fabrication and electrochemical characterization of truncated cone-shaped nanopore electrodes are reported. A nanopore electrode is a Pt disk electrode embedded at the bottom of a conical pore, the circular orifice of the pore having nanometer dimensions. The electrochemical properties of nanopore electrodes with orifice radii of 39 and 74 nm are presented. Both the steady-state and transient voltammetric behavior of the nanopore electrode are reported and compared to predictions obtained using finite-element simulations. The truncated cone-shaped pore electrode possesses a unique transport property—the steady-state flux of molecules into a deep pore is limited by the restriction near the pore orifice, and thus, the steady-state current is independent of the pore depth. This characteristic is potentially useful in studying transport through nanometer-scale orifices.

We report the fabrication and electrochemical characterization of the truncated cone-shaped nanopore electrode (for brevity, hereafter referred to as a "nanopore electrode"). Fabrication of the nanopore electrode, schematically depicted in Figure 1,

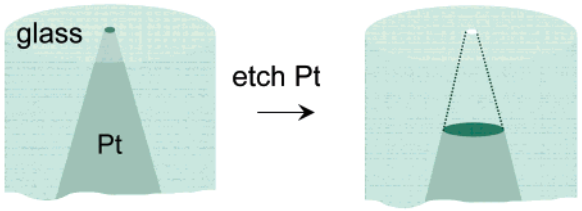

Figure 1. Fabrication of a nanopore electrode.

involves three steps: (1) sealing an atomically sharp Pt wire in a glass capillary; (2) polishing the capillary until a Pt disk of nanometer dimensions is exposed; and (3) electrochemically etching the exposed Pt to produce a truncated cone-shaped nanopore in glass, the bottom of the pore defined by a Pt disk electrode.

Our interest in the nanopore electrode is in developing a structurally simple and reliable platform for investigating molecular transport through orifices of nanoscale dimensions. Recent reports in molecular biology and analytical chemistry have led to a new class of molecular sensors based on transport in biological and artificial pores of nanometer dimensions.[1−25] Studies of pore transport at nanometer dimensions have employed free-standing membranes containing either an individual pore or many pores. By free standing, we refer to membranes, either stiff or flexible, that are mounted in a cell such that solution is able to freely contact both sides of the membrane, while the membrane edges are mechanically supported. This approach includes studies of protein ion channels inserted in lipid membranes[8,12−17,20−24] as well as synthetic pores.[1−7,9−11,18,19,25] Membranes with a single pore of diameter (d_p) less than 100 nm have been fabricated recently in track-etched polycarbonate membranes ($d_p = 2$ nm)[26] and in ion-milled Si_3N_4 membranes ($d_p = 5$ nm).[18,19] Single pore membranes of larger pore dimensions have also been constructed using a single multiwall carbon nanotube ($d_p = 130$ nm) mounted in a poly(dimethylsiloxane) (PDMS) membrane[3] or using micromolding techniques to embed pores ($d_p \sim 200$ nm) in PDMS.[25]

In contrast to free-standing membranes, a nanopore electrode is open to solution though a single orifice. The advantages of this design include the following: (1) simplicity and reproducibility of fabrication; (2) a built-in signal transduction element (the Pt electrode) for monitoring molecular transport through the pore;

* Corresponding author: (e-mail) white@chem.utah.edu.

(1) Liu, N.; Dunphy, D. R.; Atanassov, P.; Bunge, S. D.; Chen, Z.; López, G. P.; Boyle, T. J.; Brinker, C. J. *Nano Lett.* **2004**, *4*, 551−554.
(2) Sun, L.; Crooks, R. M. *J. Am. Chem. Soc.* **2000**, *122*, 12340.
(3) Ito, T.; Sun, L.; Crooks, R. M. *Anal. Chem.* **2003**, *75*, 2399.
(4) Ito, T.; Sun, L.; Crooks, R. M. *Chem. Commun.* **2003**, 1482.
(5) Jirage, K. B.; Hulteen, J. C.; Martin, C. R. *Science* **1997**, *278*, 655.
(6) Harrell, C. C.; Lee, S. B.; Martin, C. R. *Anal. Chem.* **2003**, *75*, 6861.
(7) Li, N.; Yu, S.; Harrell, C. C.; Martin, C. R. *Anal. Chem.* **2004**, *76*, 2025.
(8) Kasianowicz, J. J.; Henrickson, S. E.; Weetall, H. H.; Robertson, B. *Anal. Chem.* **2001**, *73*, 2268.
(9) Lyon, W. A.; Nie, S. *Anal. Chem.* **1997**, *69*, 3400.
(10) Cannon, D. M., Jr.; Kuo, T.-C.; Bohn, P. W.; Sweedler, J. V. *Anal. Chem.* **2003**, *75*, 2224.
(11) Kuo, T.-C.; Cannon, D. M., Jr.; Chen. Y.; Tulock, J. J.; Shannon, M. A.; Sweedler, J. V.; Bohn, P. W. *Anal. Chem.* **2003**, *75*, 1861.
(12) Gu, L. Q.; Cheley, S.; Bayley, H. *Science* **2001**, *291*, 636.
(13) Kasianowicz, J. J.; Brandin, E.; Branton, D.; Deamer, D. W. *Proc. Natl. Acad. Sci. U.S.A.* **1996**, *93*, 13770.
(14) Vercoutere, W.; Winters-Hilt, S.; Olsen, H.; Deamer, D.; Haussler, D.; Akeson, M. *Nat. Biotechnol.* **2001**, *19*, 248.
(15) Howorka, S.; Cheley, S.; Bayley, H. *Nat. Biotechnol.* **2001**, *19*, 636.
(16) Movileanu, L.; Howorka, S.; Braha, O.; Bayley, H. *Nat. Biotechnol.* **2000**, *18*, 1091.
(17) Bates, M.; Burns, M.; Meller, A. *Biophys. J.* **2003**, *84*, 2366.
(18) Li, J.; Stein, D.; McMullan, C.; Branton, D.; Aziz, M. J.; Golovchenko, J. A. *Nature* **2001**, *412*, 166.
(19) Li J.; Gershow, M.; Stein, D.; Brandin, E.; Golovchenko, J. A. *Nat. Mater.* **2003**, *2*, 611.
(20) Bayley, H.; Martin, C. R. *Chem. Rev.* **2000**. *100*, 2575.
(21) Bayley, H.; Cremer, P. S. *Nature* **2001**, *413*, 226.
(22) Deamer, D. W.; Branton, D. *Acc. Chem. Res.* **2002**, *35*, 817.
(23) Nakane, J. J.; Akeson, M.; Marziali, A. *J. Phys.: Condens. Matter* **2003**, *15*, R1365.
(24) Meller, A. *J. Phys.: Condens. Matter* **2003**, *15*, R581.
(25) Saleh, O. A.; Sohn, L. L. *Nano Lett.* **2003**, *3*, 37.
(26) Siwy, Z.; Gu, Y.; Spohr, H. A.; Baur, D.; Wolf-Reber, A.; Spohr, R.; Apel, P.; Korchev, Y. E. *Europhys. Lett.* **2002**, *60*, 349.

10.1021/ac049288r CCC: $27.50
Published on Web 09/14/2004

and (3) the portability and mechanical robustness of the solid electrode (in contrast to membranes that are mounted in diffusion cells). Each of these advantages is demonstrated in this preliminary report using nanopore electrodes with pore orifices of 39- and 74-nm radii.

The nanopore electrode is related to "recessed microdisk electrodes"[27−29] and "lagoon electrodes"[27,30,31] that have been previously considered in electroanalytical applications,[32,33] as well as serving as models of structured electrode interfaces.[34] A recessed micodisk electrode is fabricated by sealing a cylindrical Au or Pt wire, of radius greater than 1 μm, in glass tubing to produce a disk electrode, followed by etching the wire to produce a pore of depth ranging from 1 to 100 μm.[28,32] The radius of the uniformly cylindrical pore is thus equal to the diameter of the wire (>1 μm). The transient and steady-state responses of recessed micodisk electrodes have been considered in detail both experimentally[28,32,33,35] and theoretically.[28,33,34] A recessed or lagoon electrode geometry has also been considered as a possible source of error in measurements of electron-transfer kinetics when using nanometer-scale electrodes,[31] as well as a means to trap single redox molecules in scanning electrochemical microscopy.[36] However, no method of fabricating electrodes of known geometry with a single nanometer-scale pore orifice has previously been reported to our knowledge.

Herein, we describe the fabrication of nanopore electrodes and provide a brief overview of both the steady-state and transient voltammetric responses of these electrodes. Finite-element analysis of the voltammetric response of a nanopore electrode is also presented. Due to the conical shape of the pore, the steady-state voltammetric current of a nanopore electrode containing a deep pore is *independent of the pore depth*. This interesting behavior is shown to be a consequence of divergent radial transport within the pore and is potentially very useful in applications investigating transport through nanometer-scale orifices.

EXPERIMENTAL SECTION

Chemicals. Ferrocene (Fc, Strem Chemical), reagent grade $CaCl_2$, NaCN, NaOH, and tetra-*n*-butylammoniumhexafluorophosphate ($TBAPF_6$, Aldrich) were used without purification. All aqueous solutions were prepared using 18 MΩ·cm water from a Barnstead E-pure water purification system. Acetonitrile (HPLC grade, J. T. Baker) was stored over 3-Å molecular sieves.

Nanopore Electrode Construction. A 2-cm-length piece of 25-μm-diameter platinum wire (Alfa-Aesar, 99.99%) was electrically contacted to a Cu wire using Ag conductive epoxy (DuPont). The Pt/Cu wire ensemble was heated in an oven at 120 °C for ∼15 min to dry the Ag epoxy.

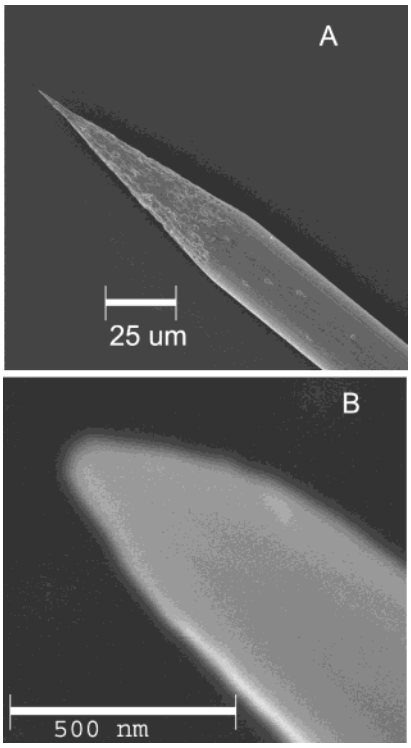

Figure 2. SEM images of a sharpened Pt wire.

The end of the Pt wire was electrochemically etched to a sharp point in either a 15% $CaCl_2$ or 6 M NaCN/0.1 M NaOH solution following standard methods reported elsewhere.[37] Briefly, an ac voltage of ∼2 V (peak to peak) was applied between the Pt wire and a large-area Pt electrode. Bubbles formed at the Pt/solution interface during electrochemical etching; the applied voltage was removed immediately upon cessation of bubbling, and the sharpened Pt wire was washed with H_2O. The end of the wire has a conical shape after etching, as demonstrated below. We found that etching the Pt wire in the $CaCl_2$ yielded tips with cone angles of ∼16°. Etching in NaCN yielded cone angles between 15° and 32°. Figure 2 shows a scanning electron micrograph (SEM) at low and high magnifications of a Pt wire etched in NaCN.

The etched Pt wire was inserted with care into a 10-cm length of glass tubing (Corning borosilicate, Pyrex-7740, 6.4-mm outer diameter, 1.0-mm inner diameter, softening point 820 °C) leaving ∼4-mm space between the tip and the end of glass tube. The glass tube was then melted around the Pt wire using a H_2/O_2 flame. An optical microscope was used to check the sealing and ensure that no air bubbles were trapped near the metal tip.

A key to the preparation of the nanopore electrode is that the shape of Pt tip does not change when it is sealed in glass. This is a reasonable expectation, as the melting point of Pt (1769 °C) is ∼1000 °C higher that the softening temperature of the glass capillary. Optical micrographs of a Pt electrode, before and after sealing in glass, obtained using an Olympus Microscope (BX60, total magnification 90×), are shown in Figure 3. No change in the tip shape at the micrometer level is observed upon sealing the wire in glass. Clearly, structural changes may occur at the very end of the tip that cannot be resolved by optical microscopy.

(27) Zoski, C. G. In *Modern Techniques in Electroanalysis*; Vanysek, P., Ed.; Wiley: New York, 1996.
(28) Bond, A. M.; Luscombe, D.; Oldham, K. B.; Zoski, C. G. *J. Electroanal. Chem.* **1988**, *249*, 1.
(29) West, A. C.; Newman, J. *J. Electrochem. Soc.* **1991**, *138*, 1620.
(30) Baranski, A. S. *J. Electroanal. Chem.* **1991**, 307, 287.
(31) Oldham, K. B. *Anal. Chem.* **1992**, *64*, 646.
(32) Henry, C. S.; Fritsch, I. *Anal. Chem.* **1999**, *71*, 550.
(33) Shao, Y.; Mirkin, M. V.; Fish, G.; Kokotov, S.; Palanker, D.; Lewis A. *Anal. Chem.* **1997**, *69*, 1627.
(34) Amatore, C.; Savéant, J. M.; Tessier, D. J. *J. Electroanal. Chem.* **1983**, *147*, 39.
(35) Tokuda, K.; Morita, K.; Shimizu, Y. *Anal. Chem.* **1989**, *61*, 1763.
(36) Fan, F.-R. F.; Kwak, J.; Bard, A. J. *J. Am. Chem. Soc.* **1996**, *118*, 9669.
(37) (a) Melmed, A. J. *J. Vac. Sci. Technol. B* **1991**, *9*, 601. (b) Melmed, A. J.; Carroll, J. J. *J. Vac. Sci. Technol. A* **1984**, *2*, 1388.

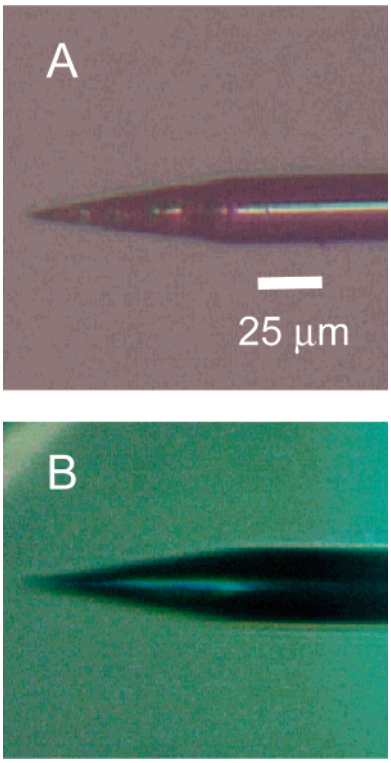

Figure 3. Optical microscopy images of an etched Pt tip (A) before and (B) after sealing it into glass.

After sealing the Pt in the glass, the Cu wire is secured to the glass capillary with insulating epoxy (Dexter). The end of the capillary containing the sealed Pt wire is polished flat with successively finer grit sandpaper (400-, 600-, and 800-grit Carbimet disks, Buehler). The thickness of the glass layer between the end of the Pt wire and the polished glass surface is periodically monitored by examining the electrode under an optical microscope. The thickness of this layer is reduced as much as possible, without exposing the Pt wire, using sandpaper. At this stage, the glass is polished using aluminum oxide powder (300 nm, Alfa Aesar, 99.99%) on a wetted felt pad. Exposure of the Pt disk during polishing is determined by measuring the steady-state voltammetric response of the electrode in an CH_3CN/0.1 M $TBAPF_6$ solution containing 5 mM Fc. The sensitivity of the potentiostat described below allows the recording of voltammograms in the Fc solution corresponding to electrodes with radii as small as 1 nm. Thus, a voltammetric response for the oxidation of Fc is observed upon any exposure of the Pt wire. Although this method requires many iterations between polishing and testing before a voltammetric response for Fc oxidation is observed, we have had a very high success rate in producing electrodes with radii less than 100 nm. Over 50 electrodes with radii ranging from 15 to 100 nm have been synthesized in our laboratory that display nearly ideal voltammetric responses, vide infra. The typical electrode preparation requires between 1 and 2 h of polishing/testing before the Pt nanodisk is exposed at the end of the electrode.[38]

To make a nanopore electrode, the nanodisk electrode was electrochemically etched in a 15% $CaCl_2$ solution (pH ~5.5) with the entire cell placed in an ultrasonic bath (Sonicor Instruments Corp., Copiague, NY, model SC-40). An ac voltage of 5 V was applied between the Pt nanoelectrode and a Pt wire counter electrode for either 10 or 20 s. The electrode was then first rinsed with water and ethanol, respectively, and sonicated in the CH_3CN solution containing 0.1 M $TBAPF_6$ and 5 mM Fc for at least 2 min before electrochemical measurements.

(38) Zhang, B.; White, H. S. *J. Electroanal. Chem.*, in preparation.

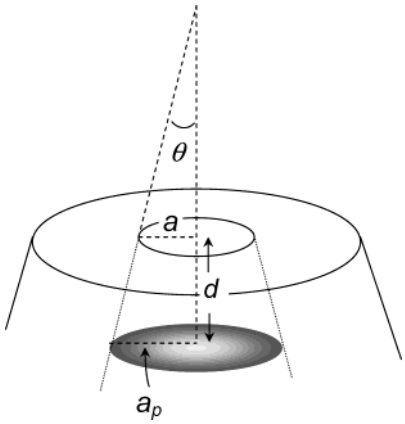

Figure 4. Nanopore electrode geometry.

Electrochemical Apparatus. A Cypress model EI-400 bipotentiostat interfaced to a computer through an AT-MIO16E-10 data acquisition board (National Instruments) was controlled via a BNC-2090 analog breakout accessory (National Instrument). Voltammetric data were recorded using in-house virtual instrumentation written in LabVIEW (National Instrument). The high-sensitivity preamplifier (0.1−10 nA/V) of the bipotentiostat was used in all experiments. A one-compartment, two-electrode cell was employed with the cell and preamplifier in a Faraday cage. A Ag/AgO or Ag/AgCl electrode was used as the reference/auxiliary electrode.

Scanning Electron Microscopy. SEM images were obtained using a Hitachi S3000-N microscope. Pt disk and nanopore electrodes were coated with an ~2-nm-thick carbon or Au layer prior to imaging.

Finite-Element Simulations. The voltammetric responses of nanopore electrodes were simulated using Femlab v2.3 software (Comsol, Inc.) operated on a Dell Dimension XPS (Pentium 4 CPU, 3.2 GHZ, 2 GB RAM).

RESULTS AND DISCUSSION

Nanopore Electrode Geometry. Before presenting experimental results, we describe the geometry of the nanopore electrode and present an overview of the strategy we have employed in determining the electrode size and shape. The geometry of a truncated cone-shaped nanopore electrode, shown in Figure 4, is fully characterized by any three of the following four parameters: the depth of the pore, d, the radius of the Pt disk at the bottom of the pore, a_p, the orifice radius, a, and the half-cone angle θ. The angle θ is determined by the cone angle of the etched Pt wire before it is sealed in glass, which is readily measured by optical microscopy to within ±1° as described in the Experimental Section. The radius of the orifice, a, is equal to the radius of the Pt nanodisk prior to etching the Pt. The latter can be readily determined from the steady-state limiting current, i_d, of the disk electrode:[39]

$$i_d = 4nFDC_b a \qquad (1)$$

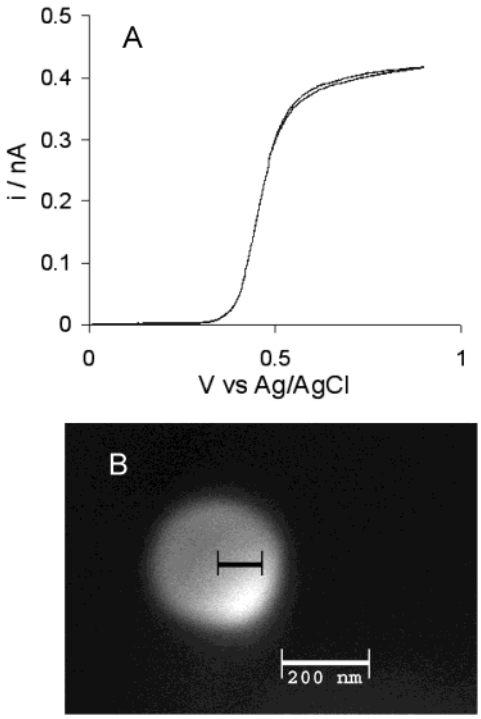

Figure 5. (A) Voltammetric response at 10 mV/s of a 91-nm-radius Pt microdisk electrode in CH_3CN/0.1 M $TBAPF_6$ containing 5 mM Fc; (B) SEM image of the same electrode. The bar drawn across the Pt disk surface corresponds to a length of 91 nm.

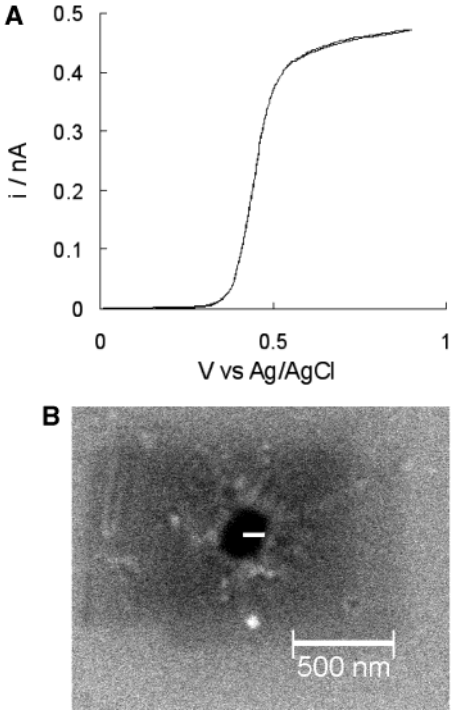

Figure 6. (A) Voltammetric response at 10 mV/s of a 102-nm-radius Pt microdisk electrode in CH_3CN/0.1 M $TBAPF_6$ containing 5 mM Fc; (B) SEM image of the pore that resulted from etching the same electrode. The bar drawn across the nanopore electrode orifice corresponds to a length of 102 nm.

In eq 1, n is the number of electrons transferred per molecule, F is Faraday's constant, and D and C_b are the diffusion coefficient and bulk concentration of the redox molecule, respectively. Values of a were determined by measuring i_d for the oxidation of 5.0 mM Fc in an CH_3CN solution containing 0.1 M $TBAPF_6$. SEM images demonstrate that the electrodes have the expected circular disk shape with radii that are typically slightly larger that the value of a determined from voltammetric measurement of i_d. For instance, Figure 5 shows an SEM image of a Pt disk of radius equal to 91, as determined from measurement of i_d (the estimated relative error in determining electrode radii is ±5%). For comparison between the electrochemical and microscopy measurements, a 91-nm-long bar has been drawn across the electrode surface in the SEM image. This level of agreement is typical of electrodes prepared by the method described in the Experimental Section.

Figure 6A shows the voltammetric response of a different Pt microdisk, from which a radius of 102 was determined. Figure 6B shows the SEM image of the pore created by etching this electrode for 10 s in the 15% (v/v) $CaCl_2$ solution. Again, a bar corresponding to the electrochemical measured radius (102 nm) is drawn across the pore orifice for comparison. The agreement between the SEM and electrochemical measured radii is excellent. Most importantly, the results indicate that the $CaCl_2$ solution does not significantly etch the pore wall, which would result in a pore radius different from the Pt disk radius prior to etching. Throughout the remainder of this report, we will assume that the value of a measured from the voltammetric limiting current for the Pt disk, *prior to etching*, is a good approximation of the pore orifice radius.

As will be demonstrated in a later section, the pore depth, d, can be determined by computational analysis of the dependence of the voltammetric response on scan rate. Alternatively, the radius of the microdisk at the bottom of the pore, a_p, may be determined directly by measuring the coulometric charge associated with the oxidation/reduction of a known quantity of redox-active molecules adsorbed on the electrode surface[40] or by coulometric analysis of the quantity of a dissolved redox molecule contained within the pore. The latter method will also be demonstrated in the results presented below.

Nanopore Electrode Voltammetry. Figure 7 shows the voltammetric response (10 mV/s) of an inlaid nanodisk electrode in a CH_3CN solution containing 5.0 mM Fc and 0.1 M $TBAPF_6$. In agreement with theory and previous results of voltammetry at nanodisk electrodes,[33] the voltammogram has a sigmoidal shape and displays no hysteresis on the reverse scan. From the voltammetric diffusion-limited current, $i_d = 340$ pA, the radius of the disk is computed using eq 1 to be 74 nm. The Pt electrode was then etched for 10 s in a 15% (m/V) $CaCl_2$ solution to create a nanopore electrode. Following etching, the nanopore electrode was rinsed with water and ethanol, respectively, and then sonicated in the CH_3CN solution containing 5 mM Fc and 0.1 M $TBAPF_6$ for at least 2 min. This last step is to ensure that the pore is filled by the CH_3CN solution. Figure 7 shows the voltammetric response (10 mV/s) of the Pt nanopore electrode in the 5.0 mM Fc solution. (The Pt wire was originally sharpened in a NaCN solution and θ measured to be equal to 16°.) The voltammetric response retains the characteristic sigmoidal shape

(39) Saito, Y. *Rev. Polarogr.* **1968**, *15*, 177

(40) Watkins, J. J.; Chen, J.; White, H. S.; Abruna, H. D.; Maisonhaute, E.; Amatore, C. *Anal. Chem.* **2003**, *75*, 3962.

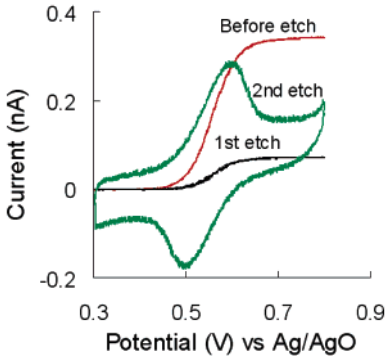

Figure 7. Voltammetric response at 10 mV/s of a 74-nm-radius nanopore electrode in CH_3CN/0.1 M $TBAPF_6$ containing 5 mM Fc before (red curve) and after the first (20 s, black curve) and second etch (20 s, green curve).

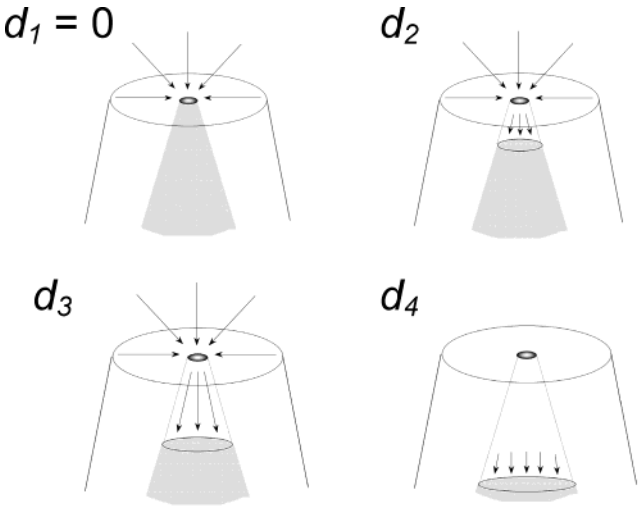

Figure 8. Schematic diagram depicting the flux of Fc with increasing pore depth ($d_1 = 0 < d_2 < d_3 < d_4$).

of a steady-state response, but the limiting diffusion current decreases to ~25% of the original value for the unetched electrode. The electrode was then removed from solution, rinsed with water, and re-etched in the $CaCl_2$ solution for an additional 10 s. The voltammetric response after the second etch, Figure 7, displays a peak-shaped voltammogram, characteristic of a "thin-layer cell" response (vide infra).[41]

The dependence of the voltammetric response on pore depth is qualitatively understood by considering the distance that molecules diffuse during the experiment, δ, relative to the pore dimensions, Figure 8. For the inlaid Pt disk (i.e., unetched electrode, $d_1 = 0$ in Figure 8), the convergent quasi-radial diffusion of the redox molecule to the electrode results in a steady-state voltammetric response at moderately slow scan rates. In this situation, the distance that molecules are transported from the bulk to the inlaid disk can be approximated as equal to $10a$,[41] or ~1 μm for the 74-nm-radius nanodisk electrode considered in Figure 7. A steady-state sigmoidal response will be observed as along as the quantity $10a$ is much smaller than the distance the redox molecule diffuses on the time scale of the voltammetric experiment, t_{expt}. The latter can be approximated by the Einstein relationship, $\delta^2 = 2Dt_{expt}$.[42] In the linear sweep voltammetric experiment, t_{expt} is given by the expression $t_{expt} = RT/\nu F$, where ν is the voltammetric scan rate and R and T are the gas constant and absolute temperature, respectively.[41] Thus, at $\nu = 10$ mV/s, $t_{expt} = 2.6$ s and $\delta = 112$ μm (assuming typical values of D (10^{-5} cm^2/s) and T (298 K)). Thus, since 112 μm $\gg$ 1 μm, a steady-state voltammogram is obtained at the unetched electrode (a more rigorous description of the steady-state nature of the microdisk response can be found in several references[27,41]).

The same qualitative arguments can be applied to transport at the nanopore electrode. When the Pt disk is etched to generate a pore in glass, the redox molecules must now diffuse the length of the pore, d, in addition to diffusing from the bulk solution to the orifice. If the sum of the pore depth (d_2 in Figure 8) plus the diffusion length outside the pore (~$10a$) is much smaller than the distance that the molecules diffuse on the time scale of the experiment, then a steady-state voltammetric response will again be observed. We will use the symbol i_d^p to designate this steady-state current (the superscript "p" indicates that the pore has a nonzero length; thus, i_d^p is always less than i_d). As the pore becomes deeper (d_3 in Figure 8), a situation develops where the current that arises from the *transient* oxidation of the molecules that are initially present in the conical pore is significantly larger than i_d^p. The oxidation of molecules initially in the pore will give rise to a symmetrical peak-shaped voltammogram analogous to the response of a thin-layer electrochemical cell.[41] This "thin-layer cell" current is superimposed on top of the steady-state current, i_d^p. Finally, when the pore depth becomes much greater than the diffusional distance (d_4 in Figure 8), then only those molecules close to the surface of the electrode at the bottom of the pore will be oxidized or reduced, and the voltammetric behavior will resemble that of a planar electrode, displaying the characteristic peak-shaped voltammetric curves with $t^{1/2}$ diffusional tailing.[41]

Inspection of Figure 7 shows that three of the responses discussed above are observed. Sigmoidal waves are observed before and after the first etch, while a peak-shaped voltammogram is observed after the second etch. The results are qualitatively consistent with the first etch producing a shallow pore and the second etch producing a significantly deeper pore. The depths of the pore after each etching will be quantitatively determined below.

t_{expt} in the above experiment was varied by a factor of 50 by varying the scan rate, ν, between 10 and 500 mV/s. Figure 9 shows the scan rate dependence of the voltammetric responses before, and after the first and second etches. A scan rate of 500 mV/s corresponds to $t_{expt} = 51$ ms and $\delta = 16$ μm, the latter quantity still significantly larger than $10a$. Thus, at scan rates of 500 mV/s, the voltammogram for the unetched Pt microdisk retains a sigmoidal shape. Similarly, the nanopore electrode after the second etch displays a peak-shaped voltammogram regardless of scan rate (only results for ν up to 50 mV/s are shown in Figure 9c), as expected, since δ is already smaller than the pore depth even at the slowest scan rate.

In contrast to the above limiting behaviors, the shape of the voltammetric response after the first etch has a significant

(41) Bard, A. J.; Faulkner, L. R. *Electrochemical Methods.* 2nd ed.; John Wiley & Sons: New York, 2001.
(42) Berg, H. C. *Random Walk in Biology*; Princeton University Press: Princeton, NJ, 1993.

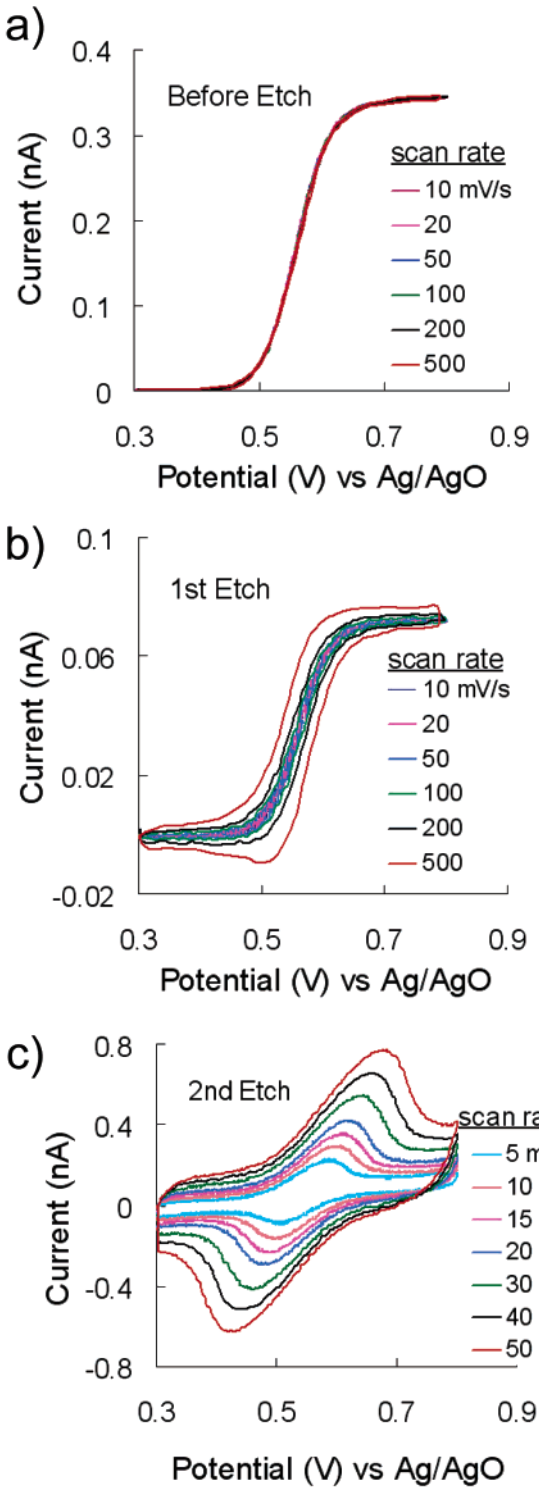

Figure 9. Voltammetric response of the 74-nm-radius nanopore electrode in CH_3CN/0.1 M $TBAPF_6$ containing 5 mM Fc (a) before and (b) after the first and (c) second 20-s etch. Scan rates are indicated on the figure.

qualitative dependence on scan rate. At slow scan rates, a steady-state sigmoidal response is observed, characteristic of the pore depth being less than the diffusion length. In contrast, at fast scan rates (>200 mV/s), the voltammogram takes on a peak shape indicative of the diffusion length approaching the pore depth. From this result, the pore depth can be approximated as being

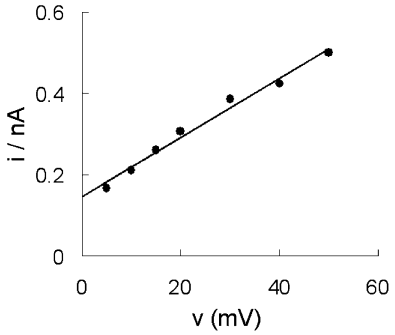

Figure 10. Voltammetric peak current plotted as a function of ν for the data shown in Figure 9c.

comparable to the diffusion length, $\delta = 16\ \mu$m. While this method of estimating the pore depth is very approximate, we will momentarily demonstrate that it yields a value that is in fact very close to the actual pore depth.

Figure 10 shows the peak current, i_p, plotted as a function of the scan rate, ν, for voltammograms recorded after the second etch, Figure 9c. As anticipated, the linear response and finite intercept suggest that the response results from both the oxidation of molecules initially within the pore and a steady-state contribution from the diffusion of molecules from the bulk to the electrode surface, i_d^p. The net current can be thus approximated by[43]

$$i_p = i_d^p + (n^2F^2\nu/4RT)C_bV_p \qquad (2)$$

where V_p is the volume of the pore. From the slope of the plot of i_p versus ν, we estimate that the pore contained 7.85×10^{-15} mol of Fc prior to the measurement ($= C_bV_p$). Using $C_b = 5$ mM, V_p is then computed to equal 1.6×10^{-9} cm^3, which, when combined with $\theta = 16°$ (or alternatively using $a = 74$ nm), yields a pore depth of 27.5 μm. The radius of the disk at the bottom of the pore is then computed to be 7.9 μm. This method cannot be employed to determine the pore depth after the first etch, because the contribution to the net current from the thin-layer effect is very small relative to i_d^p. However, computer simulations of the voltammetric response (presented in a later section) can be used to extract the pore geometry for any pore depth.

A significant background capacitive current and ohmic potential loss are evident in the voltammetric responses of the nanopore electrodes (Figure 9c). The ohmic potential loss results in a large splitting of the anodic and cathodic waves that prevents recording the voltammetric response at very high scan rates. However, at sufficiently high scan rates, and in the absence of ohmic resistance, the voltammetric current at any nanopore electrode would be controlled solely by planar diffusion in the solution adjacent to the Pt surface (see Figure 8, corresponding to d_4).

The increased capacitance after etching the electrode to create a nanopore is due to the increased area of exposed Pt and, thus, the corresponding increase in the capacitance of the Pt/solution interface. For instance, upon etching the 27.5-μm-deep pore in the 74-nm-radius microdisk, the active area of the Pt electrode increases by over 5 orders of magnitude (from 1.7×10^{-10} to 2.3

(43) This simple relationship is accurate to within ~3%, as determined by finite-element simulations to be reported elsewhere.

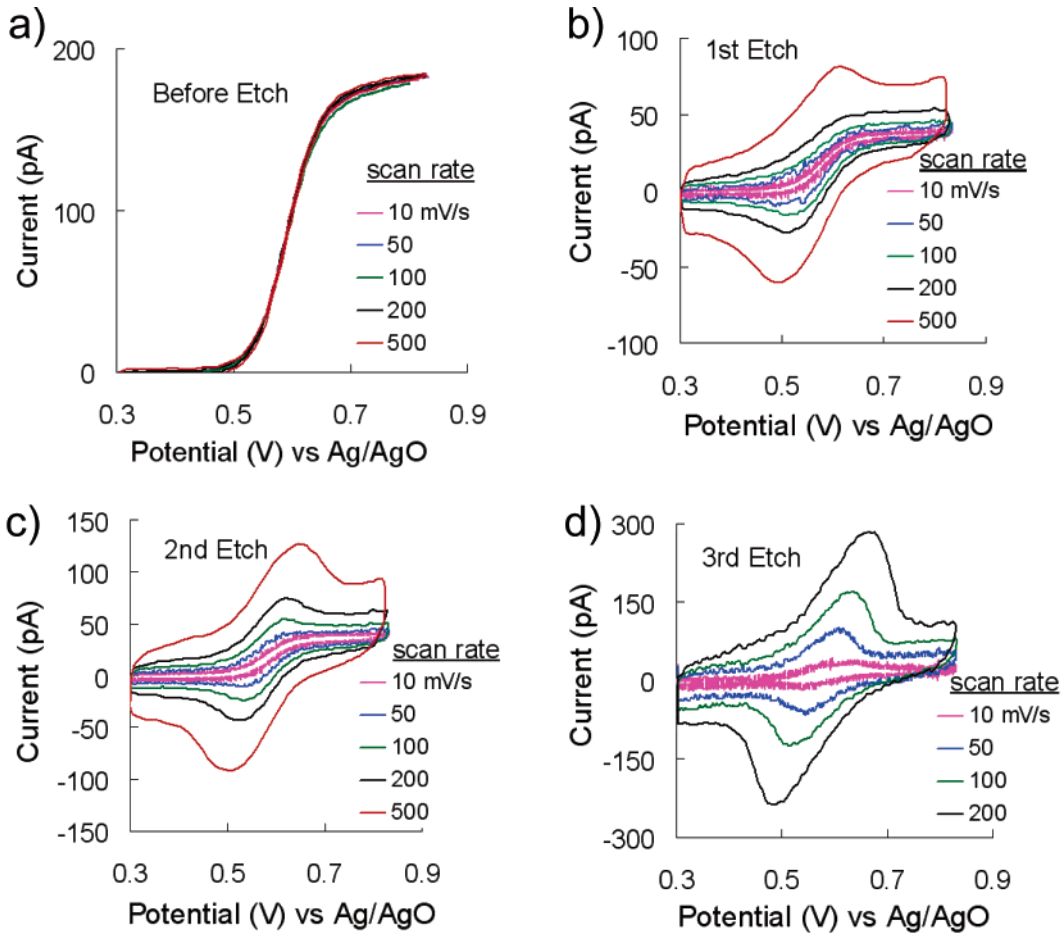

Figure 11. Voltammetric response of a 39-nm-radius Pt disk electrode in CH_3CN/0.1 M $TBAPF_6$ containing 5 mM Fc (a) before and (b)−(d) after three successive etches, each for 10 s. Scan rates are indicated on the figure.

$\times 10^{-5}$ cm^2). Assuming a Pt/0.1 M KCl interfacial capacitance of 10 μF/cm^2 yields a net electrode capacitance of 2.3×10^{-10} F. Thus, at a scan rate of 0.05 V/s, the background capacitive current ($= \nu C$) is expected to be ~0.1 nA. This prediction is in good agreement with the capacitive currents presented in Figure 9c. The ohmic potential loss results from the flow of ionic charge, generated by both the faradaic and capacitive currents, through the narrow pore.

The ohmic potential loss is expected to increase with increasing pore depth, again a consequence of the increase in the active Pt area with increasing pore depth, which results in increased faradaic and capacitive currents. The resistance of the pore also increases with pore depth, but as shown in the following sections, the dependence of transport resistance on pore depth is very weak.

Figure 11 shows the scan rate dependence of a different electrode before and after three etches, each for 10 s. The radius of the microdisk before etching was determined from the voltammetric response to be 39 nm. Qualitatively, the dependence of the voltammetric response on the pore depth (deeper after each etch) and scan rate is the same as for nanopore electrode with the 74-nm orifice. Faster scan rates and a deeper pore result in peak-shaped voltammograms, characteristic of the transition from steady-state pore diffusion to a thin-layer cell behavior. Slow scan rates and shallow pores result in steady-state sigmoidal voltammograms.

Finite-Element Simulations of the Voltammetric Response. Description of the Model and Computation. In this section, we describe finite-element simulations of the voltammetric response of the nanopore electrode. No restrictions are placed on scan rate or pore geometry, and results for both transient (fast scan) and steady-state (slow scan) voltammetric behaviors are presented. The results of the simulations will be compared directly to the experimental voltammograms (Figures 9 and 11) to demonstrate the accuracy of determining the pore geometry by the methods described above. Figure 12 shows the model used in our simulations. The nanopore electrode is modeled using a cylindrical coordinate system, the origin ($z = 0$, $r = 0$) corresponding to the center of the orifice. Simulations were performed using Femlab (see Experimental Section for machine and software details, and the Supporting Information file for addition simulation details).

We assume that transport is due solely to diffusion and that the electron-transfer reaction is reversible. These are reasonable assumptions for the voltammetric oxidation of 5 mM Fc at Pt (at $\nu = 0.5$ V/s or slower) in a solution containing 0.1 M supporting electrolyte.

We modeled a reversible 1-e oxidation, $R \rightarrow O + e^-$, with the assumption that the diffusivities of O and R are equal. To approximate the semi-infinite boundary condition of the experiment, the boundary of the bulk solution in the model was extended

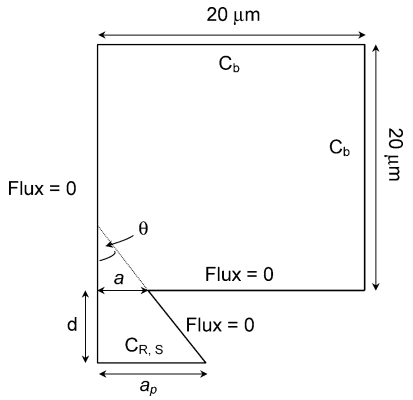

Figure 12. Model of the nanopore electrode used in finite-element simulations and corresponding boundary conditions.

to a distance 20 μm away from the orifice center in both the r and z directions. This distance is ~250× larger than the largest pore orifice (74 nm) considered in this report. The boundary of the bulk solution was held at a fixed concentration, C_b (= 5 mM). The fluxes at the glass surfaces (exterior and interior to the pore) were set equal to zero, as well as the flux on the centerline axis.

The concentration of the reactant (species R) and product (species O) at the electrode surface are designated as $C_{R,s}$ and $C_{O,s}$. From the Nernst equation, $E = E° + (RT/nF) \ln[C_{O,s}/C_{R,s}]$, and mass balance, $C_{O,s} + C_{R,s} = C_b$ (which implies equal diffusivities of R and O), the concentration of R at the electrode is given by

$$C_{R,s} = C_b\left[\exp\left[\frac{nF}{RT}(E^o - E)\right]/\left(1 + \exp\left[\frac{nF}{RT}(E^o - E)\right]\right)\right] \quad (3)$$

In eq 3, E is the electrode potential and $E°$ is the voltammetric half-wave potential. All other parameters have been previously defined.

An infinite-Fourier series was used to model the triangular-shape potential waveform of the cyclic voltammetric experiment. In eq 4, t is time, t_0 is the period

$$E(t) = \left(\frac{\nu t_o + 2E_i}{2}\right) + \sum_n -\frac{4\nu t_o}{n^2\pi^2}\cos\left(\frac{n\pi t}{t_o}\right) \quad (4)$$

($t_0 = 0.5/\nu$), E_i is the initial potential of the scan, and n are odd-valued integers. Performing the summation over $n = 1-15$ was found to be satisfactory in generating the triangular-shaped potential function. Simulations were run with relative and absolute tolerances of 10^{-5}. Analogous Femlab simulations of the voltammetric response of hemispherical microelectrodes were found to be in excellent agreement (error less than 1%) with simulated voltammograms obtained using alternative software (DigiSim, Bioanalytical Systems).

Results and Comparison to Experimental Voltammograms. Figures 13 and 14 show simulation results that correspond to the experimental voltammograms presented in Figures 9 and 11. The shapes of the simulated voltammograms are solely a function of the nanopore geometry and scan rate. We used values of a determined, as previously described, from the limiting current of the unetched electrode (74 and 39 nm) and the measured value

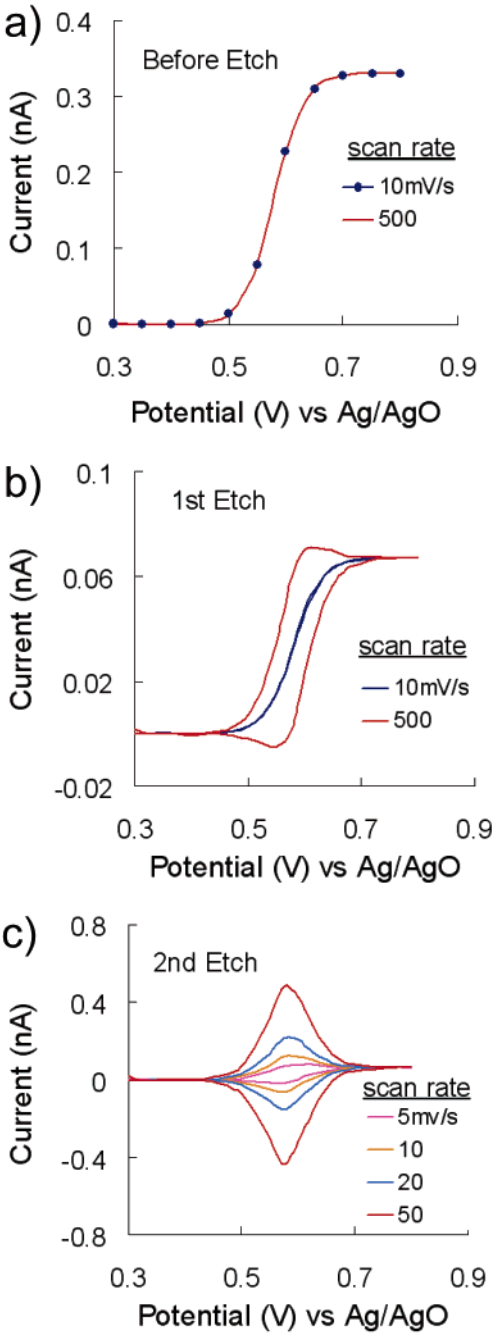

Figure 13. Simulated voltammetric response of the 74-nm-radius nanopore electrode before and after etching. The parameters a = 74 nm and $\theta = 16°$ were held constant in all simulations, while the pore depth was varied. (a) Before etching, $d = 0$; (b) after first etch, $d = 5$ μm; (c) after second etch, $d = 28$ μm. For ease of comparison, the simulated results are plotted using the same current and potential scales employed in plotting the corresponding experimental data in Figure 9.

of half-cone angle, θ (16° and 15 ± 1°, repsectively). The final geometrical parameter, d (pore depth), was adjusted in the simulation until a good fit between experiment and simulation was obtained. The capacitive current and ohmic potential drop were not considered in the simulations and thus, or course, were not reflected in the simulated voltammograms.

The simulated voltammograms in Figures 13 and 14 are plotted on the same current and potential scales as the experiment results

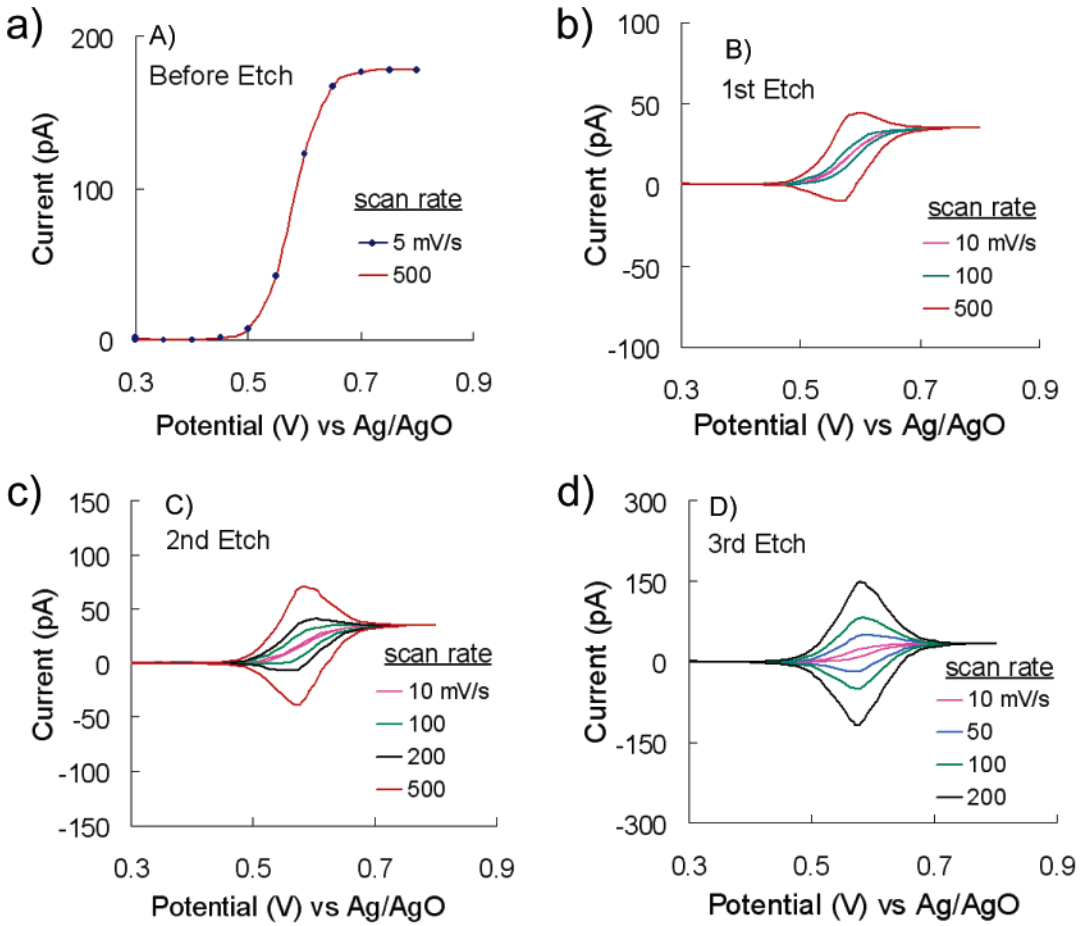

Figure 14. Simulated voltammetric response of a 39-nm-radius nanopore electrode before and after etching. The parameters $a = 39$ nm and $\theta = 15°$ were held constant in all simulations, while the pore depth was varied. (a) Before etching, $d = 0$; (b) after first etch, $d = 5$ μm; (c) after second etch, $d = 6.5$ μm, (d) after third etch, $d = 12$ μm. For ease of comparison, the simulated results are plotted using the same current and potential scales employed in plotting the corresponding experimental data in Figure 11.

in Figures 9 and 11, allowing easy visual comparison. Inspection of these figures shows that the simulations capture all features of the experimental voltammograms with semiquantitative agreement. In computing the voltammograms for the nanopore electrode with the 74-nm orifice, we used $d = 0$, 5, and 28 μm, respectively, for the unetched electrode, and for the nanopore electrode after the first and second etches, respectively. The latter value of 28 μm is nearly identical to the value of 27.5 μm obtained from the scan rate dependence (Figure 10). Values of $d = 0$, 5, 6.5, and 12 μm were used to compute the simulations (Figure 14) for comparison to the experimental results obtained using the 39-nm-radius nanopore electrode (Figure 11).

A future report will describe details of the dependence of the voltammetric response on each geometrical parameter of the nanopore electrode. We note here that simulated peak currents (at high-scan rates and for deep pores) are very sensitive to the value of d chosen in computing the voltammetric curve, moderately sensitive to θ, and weakly sensitive to a. This is a reasonable result, as the magnitude of the peak-shaped voltammogram is proportional to the volume of the pore. Conversely, the steady-state current at low-scan rates is sensitive to a and θ but nearly independent of the pore depth for very deep pores ($d \gg a$). The insensitivity of the steady-state response to d is due to the divergent flux of the molecules as they diffuse from the orifice down the pore. This is readily demonstrated by considering the steady-state diffusional mass-transport resistance, R_{MT}(cm^3/s), of a cone-shaped pore, eq 5,

$$R_{MT} = d/[\pi Da(a + d \tan \theta)] \quad (5)$$

which, in the limit $d \rightarrow \infty$, reduces to

$$R_{MT} = (\pi Da \tan \theta)^{-1} \quad (6)$$

Inspection of eq 6 shows that R_{MT} is independent of pore depth. Thus, the analysis of the steady-state flux through a deep conical nanopore does not require precise knowledge of d. For comparison, the steady-state flux in a deep cylindrical pore electrode is inversely proportional to the pore depth, approaching zero for long pores.[33,34]

Since θ and a are measured relatively easily, and since the fast-scan voltammetric response is strongly dependent on d, the geometry of the nanopore electrode can be completely characterized by a few simple measurements. One concern of our analysis is the assumption that the orifice radius is the same as the radius of the nanodisk prior to etching the electrode to generate a pore. The concern here is that the glass is etched during the etching of the Pt. We have found no evidence that this occurs when etching the Pt nanodisk in the $CaCl_2$ solution (vide supra).

However, etching the Pt in a basic NaCN solution clearly results in an orifice radius that is larger than the original microdisk radius, as determined from voltammetric analyses. Thus, care must be taken in choosing the etching solution used to generate the pore.

Conclusions. The fabrication and electrochemical characterization of truncated cone-shaped nanopore electrodes has been described. Electrodes with pore orifice radii less than 100 nm are relatively straightforward to fabricate using equipment and materials commonly found in the laboratory. While the present analysis has focused on the detailed characterization of two nanopore electrodes with 74- and 39-nm-radii orifice, we have also fabricated electrodes with significantly smaller orifices (∼15 nm). The electrochemical properties of these smaller nanopore electrodes are complicated by interactions of the pore surface with solution species, and will be the topic of a forthcoming publication.

We have demonstrated that the nanopore electrode can be well characterized using straightforward electrochemical and computational methods. Thus, these electrodes appear very well suited for fundamental studies of transport in small pores. The divergent flux of molecules as they pass through the orifice of the truncated cone-shaped pore, *in both directions*, results in the overall steady-state pore resistance being dominated by the resistance of the pore orifice. This feature may be especially useful in studying factors that control transport through nanoscale orifices.

ACKNOWLEDGMENT

This research was supported by the Defense Advanced Research Projects Agency.

SUPPORTING INFORMATION AVAILABLE

Details of the finite-element simulation of the voltammetric response of the nanopore electrode. This material is available free of charge via the Internet at http://pubs.acs.org.

Received for review May 14, 2004. Accepted August 6, 2004.

AC049288R